Biomimetic Biphasic 3-D Nanocomposite Scaffold for Osteochondral Regeneration

Nathan J. Castro and Christopher M. O'Brien
Dept. of Mechanical and Aerospace Engineering, The George Washington University, Washington, DC 20052

Lijie Grace Zhang
Dept. of Mechanical and Aerospace Engineering, Dept. of Medicine, The George Washington University, Washington, DC 20052

DOI 10.1002/aic.14296
Published online December 10, 2013 in Wiley Online Library (wileyonlinelibrary.com)

Scaffold-based interfacial tissue engineering aims to not only provide the structural and mechanical framework for cellular growth and tissue regeneration, but also direct cell behavior. Due to the disparity in composition of the osteochondral (cartilage and bone) interface, this work has developed a novel biomimetic biphasic nanocomposite scaffold integrating two biocompatible polymers containing tissue-specific growth factor-encapsulated core–shell nanospheres. Specifically, a poly(caprolactone) (PCL)-based bone layer was successfully integrated with a poly(ethylene glycol) (PEG) hydrogel cartilage layer. In addition, a novel nanosphere fabrication technique for efficient growth factor encapsulation and sustained delivery via a wet coaxial electrospray technique was developed. Human bone marrow mesenchymal stem cell (hMSC) adhesion, osteogenic, and chondrogenic differentiation were evaluated. Our in vitro results showed significantly improved hMSC adhesion and differentiation in bone and cartilage layers, respectively. Studies have demonstrated promising results with novel biphasic nanocomposite scaffold for osteochondral tissue regeneration, thus, warranting further studies. © 2013 American Institute of Chemical Engineers *AIChE J*, 60: 432–442, 2014
Keywords: osteochondral, core–shell nanosphere, growth factor, biomimetic, scaffold

Introduction

Osteochondral defects, caused by osteoarthritis and trauma, present a common and serious clinical problem. For instance, osteoarthritis affects 48 million Americans and is projected to affect 67 million Americans by 2030, making it a leading cause of disability in American adults.[1,2] Osteochondral defects compromise the full thickness of articular cartilage, beyond the calcified zone, and into the subchondral bone.[3] Specifically, the articular cartilage is relatively avascular, contains few native mature cells (chondrocytes) as well as exhibits a gradient of properties from the synovial surface to the subchondral bone.[4,5] These characteristics are distinctly different from the highly vascularized and heavily cell populated composition of bone leading to a complex interface between cartilage and subchondral bone. To date, interfacial osteochondral tissue is notoriously difficult to regenerate due to this inherent complex stratified soft/hard tissue structure and poor inherent regenerative capacity.[3] No current available treatment methods provide a perfect solution. As a result, the development of novel biomimetic osteochondral tissue substitutes is of pressing interest.

Interfacial tissue engineering (ITE) holds great promise for the development of novel therapeutic approaches to address the complex nature of osteochondral defects where interfaces have shared characteristics of the tissues being connected but also contain regions of distinct composition and biological function.[6,7] Recent work has focused on the fabrication of stratified and graded scaffolds with incorporated morphogenic factors for expedited *de novo* tissue formation.[7–10] For example, Dormer et al. have developed a series of graded polymeric macrosphere-based scaffolds containing chondrogenic/osteogenic growth factors[11] and inorganic hydroxyapatite.[12] These studies helped to substantiate the importance of the presence and sustained delivery of biological factors for *in situ* tissue remodeling and formation. Moreover, it is important to note that natural human osteochondral tissue extracellular matrix (ECM) is nanometer in dimension composed of many nanostructured components (e.g., nanocrystalline hydroxyapatites, collagen and various other proteins).[13,14] However, current studies in the development of biomimetic nano osteochondral constructs integrating two distinct tissues within certain biological and mechanical constraints are very limited.[3,15–17] Thus, the objective of this study is to develop an innovative biphasic nanocomposite scaffold to provide both sustained biological cues and display biomimetic nanofeatures for enhanced human bone marrow-derived mesenchymal stem cell (hMSC) differentiation and osteochondral tissue formation.

In particular, two primary novel features delineate this work from work currently being conducted: the first novel

This article was nominated by Dr. Thomas J. Webster (Dept. of Chemical Engineering, Northeastern University) as the Best Presentation in the session "Nanostructured Scaffolds for Tissue Engineering" of the 2012 AIChE Annual Meeting in Pittsburgh, PA.

Correspondence concerning this article should be addressed to L. G. Zhang at lgzhang@gwu.edu.

feature of the biphasic osteochondral scaffold is the use of coaxial wet electrospraying for the manufacture of bone morphogenic protein-2 (BMP-2) and transforming growth factor-β1 (TGF-β1) core–shell nanospheres for sustained osteogenic and chondrogenic MSC differentiation, respectively. This technique allows for the use of a wide range of biodegradable polymers with minimized organic/aqueous phase interaction leading to greater retention of biological activity through mitigating direct exposure of biological components to harmful organic solvents.[18] Although traditional micro/nanosphere fabrication techniques have exhibited positive results, initial burst and uncontrolled release rates have restricted their full clinical potential partially due to particle size disparities which are not only limited to synthetic polymer systems, but those involving naturally-derived substituents.[19] The coaxial wet electrospray technique employed herein is expected to produce nanospheres with good size distribution resulting in minimal burst and more controlled release. In addition, nanocrystalline hydroxyapatites will be also embedded into the subchondral bone layer to further create a biomimetic nanoenvironment.

Second, a photocurable coporogen system was used to fabricate the biphasic nanocomposite constructs as a means of physically and chemically linking two distinctly different biomaterials, poly(caprolactone) (PCL) and poly(ethylene glycol) (PEG). Through the fabrication of nanospheres composed of a secondary polymeric material, we were able to address initial burst release concerns and exhibit greater sustained growth factor release. Therefore, the main caveat of our system which distinguishes it from existing literature is the sustained delivery of tissue-specific growth factors through the combinatorial effects of novel core–shell nanospheres embedded within a secondary polymer matrix leading to a novel photocrosslinkable biphasic nanocomposite osteochondral scaffold for directed and enhanced hMSC osteochondral differentiation.

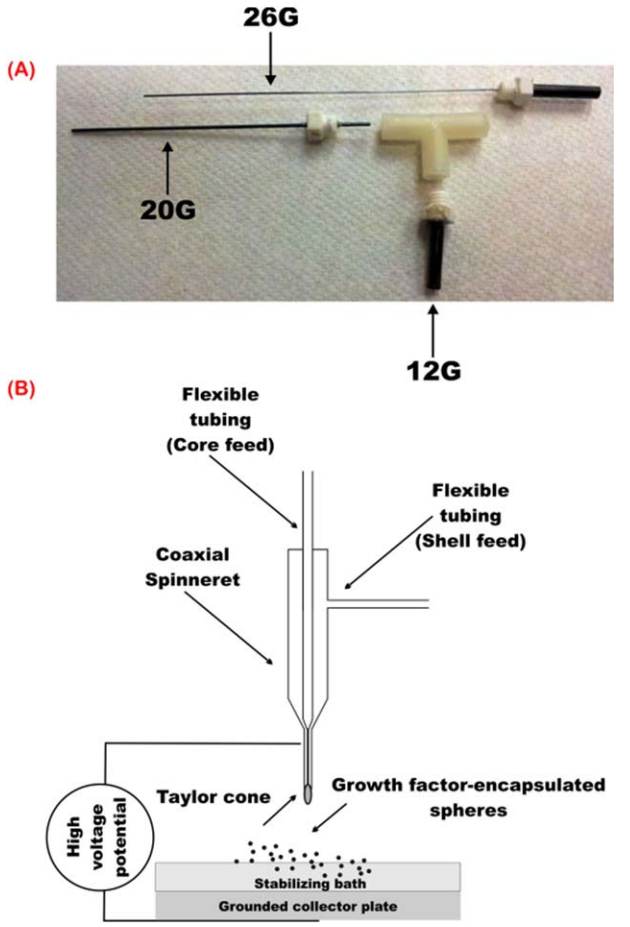

Figure 1. A coaxial electrospray system used in the manufacture of growth factor encapsulated polymeric nanospheres.

[Color figure can be viewed in the online issue, which is available at wileyonlinelibrary.com.]

Materials and Methods

PLGA/PDO wet electrosprayed nanosphere fabrication and characterization

Poly(dioxanone) (PDO) (Sigma-Aldrich, St. Louis, MO) and poly(lactic-*co*-glycolic) acid (PLGA) (Lactel Absorbable Polymers, Birmingham, AL) nanospheres were fabricated by co-axial wet electrospray via a custom coaxial needle system as shown in Figure 1A composed of a 26G inner needle (304SS 0.018″ OD, 0.01″ID) receded within a 20G needle (304SS 0.036″ OD, 0.0275″ ID) (McMaster-Carr, Robbinsville, NJ 08691).

Briefly, BMP-2 and TGF-β1 (PeproTech, Rocky Hill, NJ) lyophilized powders were resuspended per manufacturer's instructions and working concentrations of 10 ng/mL were used in all experiments. For BMP-2 encapsulated PDO nanospheres, a 2.5% (wt %) solution of PDO in 1,1,1,3,3,3-hexafluoropropanol (HFIP) (Sigma-Aldrich, St. Louis, MO) was fed through the shell feed inlet (Figure 1b) at a flow rate of 4.0 mL/h. BMP-2 was fed through the core feed inlet at the same flow rate. Voltage was adjusted during collection to prevent fiber formation and maintain adequate Taylor cone morphology. Similarly, TGF-β1 encapsulated PLGA nanospheres were fabricated using the same concentrations and flow rates wherein acetone was used as the solvent.

PDO nanospheres were collected in a chloroform stabilizing bath to assist in the prevention of agglomeration and replenished periodically during electrospraying. PLGA nanospheres were collected in an ultrapure water stabilizing bath. After collection, the baths were transferred to centrifuge tubes and ultrasonicated for 30 s (Ultrasonicator, QSonica, Newtown, CT). Emulsified samples were then immediately frozen and lyophilized for 24 h to remove the stabilizing bath before use.

Synthesized core–shell growth factor encapsulated nanosphere morphology was characterized by transmission electron microscope (TEM). Particle size analysis of nanospheres was conducted with ImageJ. Briefly, a calibrated TEM micrograph was imported in to the software and converted to a binary image with adjusted threshold to remove noise and background. Particle analysis of the binary image was conducted and particle diameters were extrapolated from calculated areas.

Encapsulation efficiency and release studies of protein encapsulated nanospheres

Release profiles of bovine serum albumin (BSA) encapsulated PDO and PLGA nanospheres were conducted. BSA is a commonly used protein employed as an easily quantifiable and reliable model for release kinetics examination. PDO and PLGA nanospheres were prepared as previously described with a working solution of 1% BSA (wt/v) in

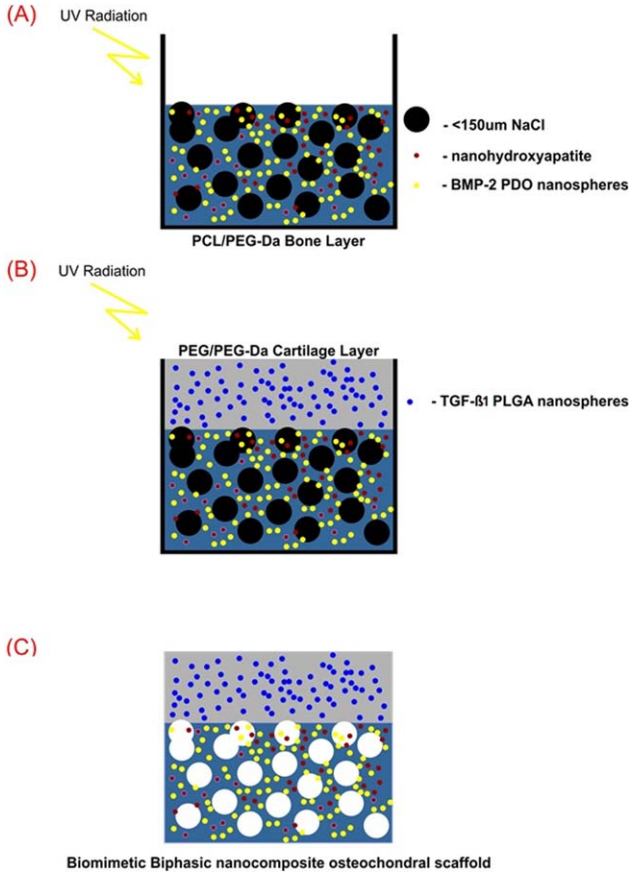

Figure 2. A photocrosslinking/co-porogen leaching method for the fabrication of biphasic biomimetic osteochondral scaffolds.

[Color figure can be viewed in the online issue, which is available at wileyonlinelibrary.com.]

ultrapure water. Lyophilized nanosphere samples were incubated in PBS under standard culture conditions for up to 18 days. Samples were pelleted and the supernatant was stored for analysis. Collected fractions and standards were analyzed spectrophotometrically (MicroBCA® Protein Kit, Fisher Thermo Scientific, Waltham, MA). Encapsulation efficiency of collected samples was analyzed by dissolving a known mass of collected sample in HFIP (PDO) and acetone (PLGA), respectively, and measuring absorbance of BSA at 280 nm.

Hydrothermally treated nanocrystalline hydroxyapatite (nHA) synthesis

A wet chemistry method plus a hydrothermal treatment as described in our previous articles[20–22] was used to synthesize nanocrystalline hydroxyapatite. Briefly, a 0.6 M ammonium phosphate (Sigma Aldrich, St. Louis, MO) solution was added to water and adjusted to a pH of 10 with ammonium hydroxide (Fisher Scientific, Pittsburgh, PA). A 1 M calcium nitrate (Sigma Aldrich, St. Louis, MO) solution was slowly titrated into the above mixture while stirring. Precipitation of HA continued for 10 min at room temperature. The solution with HA amorphous precipitate was treated hydrothermally at 200°C for 20 h in a 125 mL Teflon liner (Parr Instrument Co., Moline, IL) to produce nHA. The resultant nHA was centrifuged and rinsed thoroughly with water then dried at 80°C for 12 h. Dried nHA was ground with a ceramic pestle and mortar and run through a <150 μm sieve. Synthesized nHA particles were gold sputter-coated and imaged via scanning electron microscopy (SEM).

Biphasic (PCL/PEG-Da) osteochondral scaffold fabrication and characterization

Biphasic osteochondral scaffolds were fabricated via a novel photo-crosslinking/co-porogen leaching method for integration of two disparate polymeric materials as illustrated in Figure 2. Scaffolds were prepared as a proof of concept and each layer was evaluated separately for respective hMSC differentiation.

Bone Layer Preparation. PCL was employed as the base bone layer material in this system. It was dissolved in an excess of chloroform to allow for efficient mixing of all composite materials with PCL resultantly constituting 38% of the total mass of the bone layer. nHA (20 wt %) was added to the dissolved PCL. Separately, a 60:40 mixture of poly(ethylene glycol) (PEG, $Mn = 300$): Poly(ethylene glycol)-diacrylate (PEG-Da, $Mn = 700$) was prepared. A photoinitiator, Bis(2,4,6-trimethylbenzoyl)-phenylphosphineoxide (BAPO) (BASF, Florham Park, NJ), with excitation in the ultraviolet (UV) range was added to the PEG:PEG-Da mixture at 0.5 wt % of PEG-Da and allowed to rest overnight for adequate dissolution. Several samples were prepared (Table 1) and used for further hMSC differentiation studies. PDO nanospheres were added to the dissolved PCL/nHA mixture. Upon complete dissolution of the photoinitiator, both PCL and PEG solutions were mixed and mechanically stirred. For hMSC differentiation experiments, complete PCL/PEG mixture was cast in to a glass Petri dish allowed to rest for 10 min and cured for 30 s under UV light. Samples of 5 mm crosslinked samples were collected with a biopsy punch and leached in ultrapure water for 3 days with periodic exchange of fresh ultrapure water.

Cartilage Layer Preparation. For more efficient layer integration, the same 60:40 PEG:PEG-Da mixture served as the base material for all cartilage layer samples. As previously described, 0.5 wt % BAPO was added to the PEG:-PEG-Da mixture and allowed to rest overnight. Lyophilized TGF-β1 encapsulated PLGA nanospheres were subsequently added and mixed for adequate dispersion within the hydrogel matrix. The hydrogel mixture was then cast in to a 9 cm glass Petri dish and UV cured for 15 s. Fabricated cartilage

Table 1. PCL Bone Layer Sample Composition

	Control	nHA	Blended BMP-2/nHA	BMP-2 spheres/nHA
PCL (wt%)	38%	38%	38%	38%
PEG:PEG-Da (wt%)	38%	38%	38%	38%
NaCl (<150 μm) (wt%)	24%	24%	24%	24%
nHA	–	20wt% of PCL	20wt% of PCL	20wt% of PCL
PDO nanospheres	–	–	–	500 μg/g of PCL
BMP-2 (10 ng/mL)	–	–	67 μL	–

Table 2. PEG-Da Cartilage Layer Sample Composition

	Control	Blended TGF-β1	TGF-β1 spheres
PEG:PEG-Da	100%	100%	100%
PLGA nanospheres	–	–	500 μg/g of PEG-Da
TGF-β1 (10 ng/mL)	–	67 μL	–

layer samples used in hMSC differentiation studies can be found in Table 2. Five mm samples of crosslinked samples were collected with a biopsy punch. Sol fraction and swelling ratios of prepared hydrogel samples were evaluated as described.[23]

Osteochondral Scaffold Fabrication. Biphasic biomimetic osteochondral scaffolds were prepared as depicted in Figure 2. Briefly, the complete PCL/PEG-Da bone layer mixture was cast in to a 9 cm glass Petri dish and allowed to rest for 5 min before partial (15 s) UV curing. The solvent (chloroform) was allowed to partially evaporate before casting of the PEG-Da cartilage layer mixture. The PEG-Da cartilage layer was cast directly on top of the partially cured PCL bone layer and UV cured for 1 min. Biphasic scaffolds were sputter-coated with gold and imaged via focused ion beam operating in SEM mode (SEM, Zeiss NVision 40 FIB, Thornwood, NY).

Bone/Cartilage Protein Release. Release profiles for each respective layer and composition were evaluated. Briefly, scaffolds containing 1 mg/mL BSA were fabricated as described in Tables 1 and 2. Samples of 5 mm ($n = 6$) were incubated in PBS at 37°C and 5% CO_2. Fractions of the supernatant were centrifuged, collected, and BSA content was measured spectrophotometrically at predetermined time points. Protein release profiles were plotted as a fraction of total encapsulated protein.

Mechanical Testing of Biphasic Nano-Osteochondral Constructs. The elastic modulus of fabricated biphasic nanocomposite scaffolds was determined via unconfined compression testing ($n = 3$) (Applied Test Systems, Butler, PA) fitted with a 500N load cell at a crosshead speed of 1.2 cm/min. Samples were collected with a 5 mm biopsy punch,

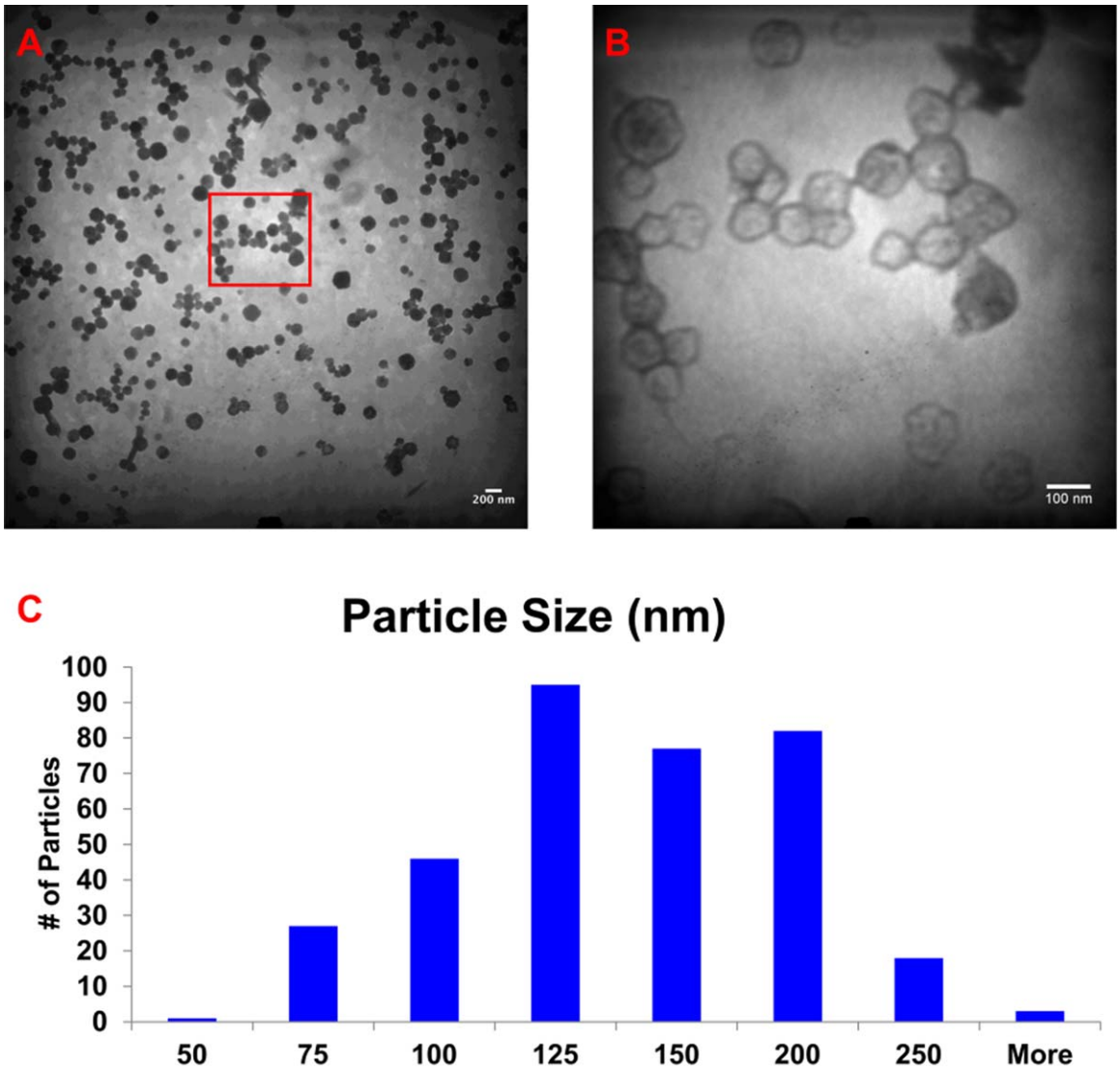

Figure 3. (A) and (B) TEM of BMP-2 encapsulated PDO nanospheres, (B) is a high-magnification image of the highlighted area, and (C) particle-size distribution results of PDO nanospheres.

PLGA spheres exhibited similar morphology and size distribution. [Color figure can be viewed in the online issue, which is available at wileyonlinelibrary.com.]

swollen for 48 h with intermittent exchange of fresh ultrapure water and blotted dry before testing.

hMSC study in vitro

Primary hMSCs were obtained from healthy consenting donors from the Texas A&M Health Science Center, Institute for Regenerative Medicine and thoroughly characterized.[24] Primary hMSCs (passage #3–6) were cultured in complete media composed of Alpha Minimum Essential medium (α-MEM, Gibco, Grand Island, NY) supplemented with 16.5% fetal bovine serum (Atlanta Biologicals, Lawrenceville, GA), 1% (v/v) L-Glutamine (Invitrogen, Carlsbad, CA), and 1% penicillin:streptomycin (Invitrogen, Carlsbad, CA) and cultured under standard cell culture conditions (37°C, a humidified, 5% CO_2/95% air environment). All of the samples were sterilized in 70% ethanol for 30 min then washed three times for 5 min in phosphate-buffered saline (PBS) before cell seeding.

hMSC Adhesion Study. Bone layer scaffolds with 0, 10, and 20% concentrations of nHA, PDO nanosphere and 20% nHA/PDO nanosphere were tested for cell adhesion. hMSCs were seeded at 50,000 cells/scaffold. The seeded scaffolds were then incubated under standard cell culture conditions for 4 h. After rinsing with PBS, the adherent cells were quantified via a CellTiter 96® AQ_{ueous} nonradioactive cell proliferation assay (MTS assay), and analyzed using a Thermo Scientific Multiskan GO spectrophotometer at a setting of 490 nm wavelength light.

hMSC Osteogenic Differentiation Study. hMSCs were seeded at a density of 10^5 cells/scaffold for osteogenic differentiation evaluation. Cell seeded bone layer scaffolds were cultured in complete media supplemented with osteogenic factors (10 nM Dexamethasone, 20 mM β-glycerophosphate, and 50 μM *L*-ascorbic acid) for 1 and 2 weeks, respectively.

Calcium deposition, one of the most important indicators of osteogenic differentiation, was measured using a calcium reagent kit (Pointe Scientific, Inc.). Briefly, hMSCs were lysed through three freeze–thaw cycles and removed. The scaffolds containing deposited calcium and ECM were immersed in a 0.6 N HCl solution at 37°C for 24 h. After the prescribed time period, the amount of dissolved calcium present in the acidic supernatant was measured by reacting with the o-cresolphthalein complexone to form a purple tinted solution. Absorbance was measured by a spectrophotometer at 570 nm. Total calcium deposition was calculated from standard curves of known calcium concentrations run in parallel with experimental groups and normalized to control scaffolds which were digested to remove the contribution of embedded nanohydroxyapatite.

Total collagen content of lysed samples was evaluated via Sircol collagen assay kit (Accurate Chemical & Scientific Corp., Westbury, NY). Per manufacturer instructions, 1 mL dye reagent was added to 100 μL lysate and shaken for 30 min. Samples were then centrifuged for 10 min at 10,000 rpm to pellet the collagen-dye complex and the supernatant was carefully decanted. Ice-cold wash reagent was used to remove unbound dye and the samples were centrifuged once more and the supernatant decanted. 250 μL alkali solution was added to solubilize the pellet and a 200 μL aliquot was transferred to a new 96-well plate and absorbance measurements were taken at 555 nm.

hMSC Chondrogenic Differentiation Study. hMSCs were seeded at a density of 10^5 cells/scaffold. Seeded scaffolds were cultured in complete media supplemented with chondrogenic factors (100 nM dexamethasone, 40 μg/mL proline, 100 μg/mL sodium pyruvate, 50 μg/mL L-Asorbic acid 2-phosphate, and 1% (v/v) ITS+) for 1 and 2 weeks, respectively. At each prescribed time point, cell seeded samples were rinsed with PBS, lyophilized, then digested in a papain digestion solution for 18 h at 60°C and stored at −80°C until analyzed. Total collagen content of digested samples was evaluated as described previously.

Glycosaminoglycan (GAG), a key component of cartilage matrix, was measured using a standard GAG assay kit (Accurate Chemical & Scientific Corp., Westbury, NY) according to manufacturer's instructions. Briefly, a predetermined volume of sample and buffer solution was added to a microcentifuge tube with 500 μL of dye reagent and mixed for 30 min. The GAG-dye complex was centrifuged for 10 min at 10,000 g until a pellet was visible. The supernatant was decanted and all residual fluid was blotted dry. Next, 600 μL of dissociation reagent was added to the tubes and shaken for 30 min; 100 μL of each solution was placed into a 96-well plate and analyzed in triplicate. Absorbance was read at 656 nm and correlated to a standard curve of known standards.

Human type II collagen was evaluated via a type II collagen ELISA assay (Fisher Scientific, Pittsburgh, PA). Briefly, control and sample aliquots were added to a precoated 96-well plate and incubated. Unbound sample was washed and a horse radish peroxidase-labeled collagen II antibody was added, incubated, and washed. After washing, tetramethylbenzidine was added producing a blue color. The reaction was stopped by the addition of an acidic stop solution and read at 450 nm.

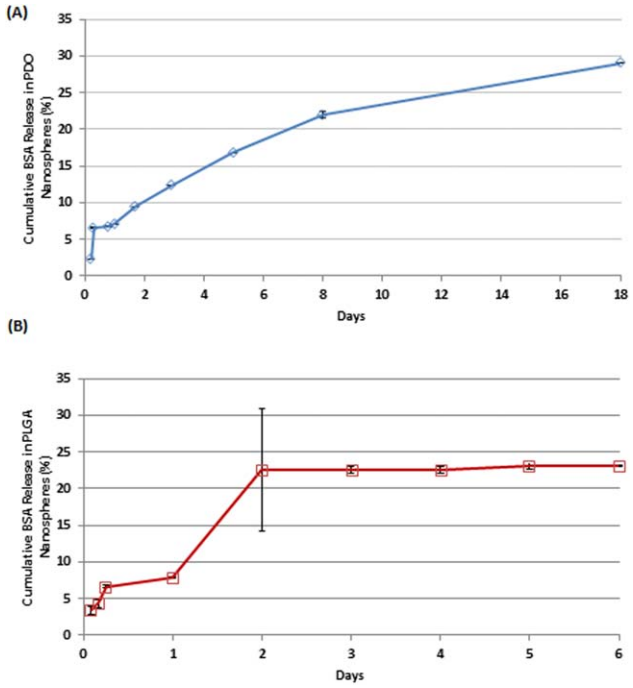

Figure 4. Release profile of (A) BSA encapsulated PDO nanospheres and (B) BSA encapsulated PLGA nanospheres.

Data are ± standard deviation, n = 6. [Color figure can be viewed in the online issue, which is available at wileyonlinelibrary.com.]

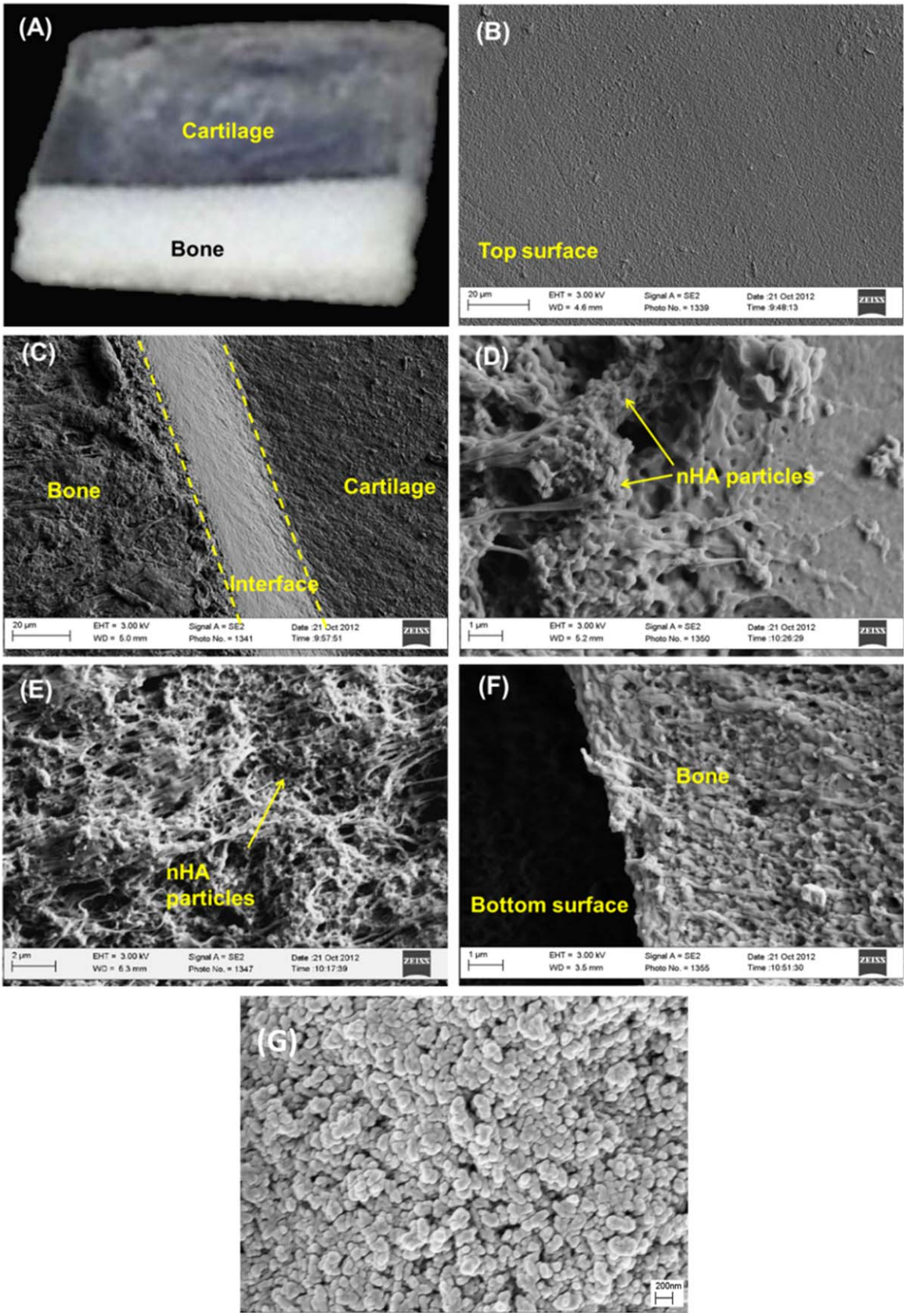

Figure 5. Optical (A) and SEM images (B–F) of biphasic biomimetic osteochondral nano scaffold, and (G) illustrates the typical SEM image of synthesized nHA particles.

[Color figure can be viewed in the online issue, which is available at wileyonlinelibrary.com.]

Table 3. Swelling Properties of Cartilage Layer Samples

	Characteristics of PEG:PEG-DA (60 wt%) hydrogels			
	Control	Blank spheres	BSA-loaded spheres	TGF-β1-loaded spheres
Swelling Ratio (%)	279.76 ± 4.92	277.73 ± 4.60	277.63 ± 3.88	170.26 ± 10.11
Sol Fraction (%)	63.71 ± 0.39	63.27 ± 0.20	63.27 ± 0.20	64.26 ± 0.87

Statistical analysis

Data are presented as the mean value ± standard error of the mean (StdEM) and were analyzed via one-way ANOVA and student's *t*-test to determine differences among the groups. Statistical significance was considered at $p<0.05$.

Results and Discussion

Nanomaterial characterization

This study synthesized and evaluated two nanomaterials, tissue-specific growth factor encapsulated core–shell nanospheres and nanocrystalline hydroxyapatite, for hMSC chondrogenic and osteogenic differentiation. Traditional emulsion-based micro/nanosphere fabrication techniques have illustrated limited control of particle size and encapsulation efficiency.[25–27] Therefore, alternative methods for the fabrication of polymeric sphere-based delivery systems have been explored which include electrospray/electrohydrodynamic techniques. Coaxial electrospraying[28] allows for easy fabrication of novel controllable core–shell nanospheres with bioactive growth factors contained within a biodegradable polymer shell exhibiting greater encapsulation (>70%) and sustained release of biological components.[29,30] Owing to these features, this work used this technique to fabricate chondrogenic and osteogenic growth-factor encapsulated PLGA and PDO nanospheres, respectively. PLGA and PDO (known commercially as PDS®, a commonly used absorbable suture[31–33]) were selected based on their excellent biocompatibility, mechanical properties and controllable degradation rates for tissue engineering and drug delivery applications.[34–41]

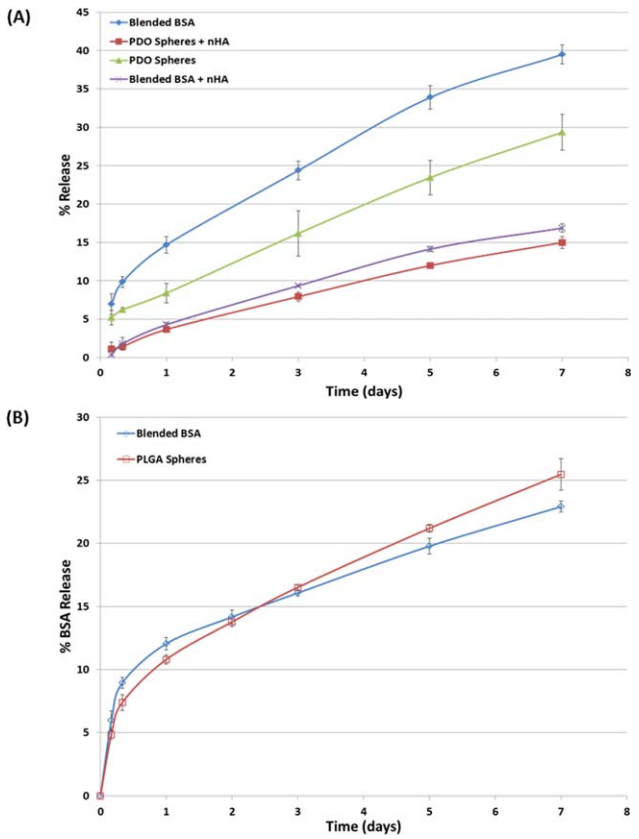

Figure 6. Release profiles of (A) bone layer scaffolds with BSA encapsulated PDO nanospheres and blended BSA, and (B) cartilage layer scaffolds with BSA encapsulated PLGA nanospheres and blended BSA.

Data are ± standard deviation, $n = 6$. [Color figure can be viewed in the online issue, which is available at wileyonlinelibrary.com.]

TEM was used to evaluate the core–shell morphology (Figure 3A,B) and particle-size distribution of synthesized PDO/PLGA nanospheres with particle sizes ranging between 75 and 250 nm with an average particle size of 150 nm (Figure 3C). The modified electrospray method employed here allows for comparable or increased encapsulation of PDO (>70%) and PLGA (>80%), respectively, where traditional emulsion methods exhibit encapsulation efficiencies of 60–80% for PLGA.[25,42–45] With respect to PDO, due to the material's relative insolubility, alternative methods for the fabrication of sustained delivery devices have been employed to include melt extrusion and thin film fabrication along with traditional emulsion techniques exhibiting encapsulation efficiencies of 26–62% for pure and copolymeric systems.[46–48] In addition, release profiles of synthesized PDO/PLGA nanospheres (Figure 4) revealed a minimized burst release within the first 8 h of incubation for both nanospheres and steady release to 18 days (PDO) and 6 days (PLGA), respectively.

Hydrothermally-treated nHA particles (Figure 5G) with biomimetic dimensions of 50–100 nm in length and 20–30 nm wide similar to natural bone mineral were synthesized and used in the current study based on its high-osteoconductive potential when used alone or in combination with other nanomaterials.[21,49,50] Therefore, our biphasic model incorporated these three specific nanomaterials for directed hMSC chondrogenesis and osteogenesis.

Biphasic (PCL/PEG-Da) osteochondral scaffold characterization and in vitro *hMSC studies*

Optical and scanning electron micrographs (Figure 5) of fabricated osteochondral scaffolds revealed excellent integration between the PEG-Da (cartilage) and PCL/PEG-Da (bone) layer. Figure 5C illustrates the UV crosslinked interface between the respective layers with higher magnification images (Figure 5D,E) further illustrating good integration. Due to the bulk crosslinking manufacturing technique employed here, a sharp transition between the respective layers was formed. An interesting feature of the fabricated osteochondral scaffold is the formation of a fibrous nanostructured network formed orthogonally to the cured surface. In addition, due to the presence of the nHA nanoparticles

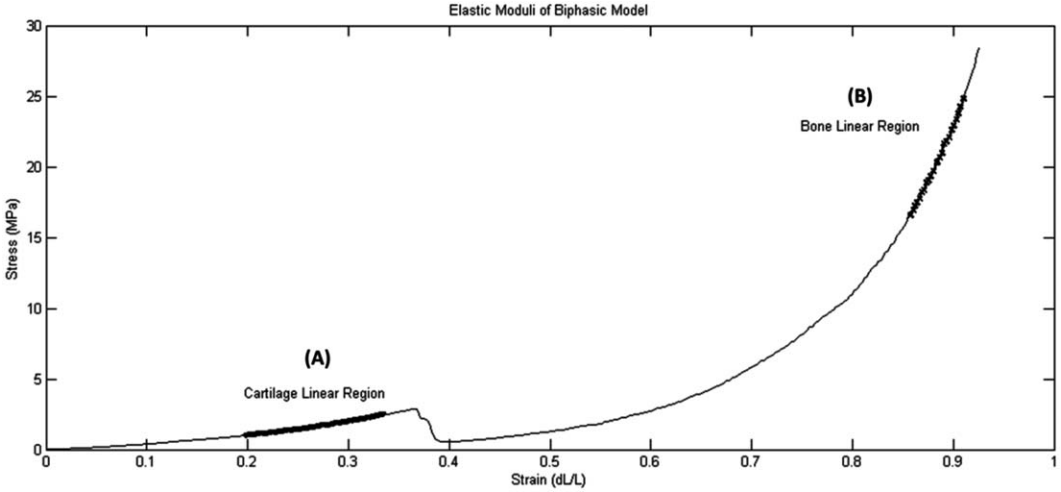

Figure 7. A stress–strain curve of the biphasic nanocomposite osteochondral scaffold.

(A) Linear region ($R^2 = 0.991$) of the cartilage layer, and (B) linear region ($R^2 = 0.996$) of the bone layer.

within the bone layer, a more biomimetic scaffold has been developed with respect to morphology and composition. In addition, a hydrogel-based cartilage matrix may allow for greater exposure of embedded PLGA nanospheres within the construct due to the materials' inherent swelling properties (Table 3) as opposed to PDO nanospheres which were embedded within a PCL matrix.

Protein release studies of the respective tissue layers were investigated to determine the release kinetics of the nanocomposite system developed here. Figure 6 shows the release profiles of blended and nanosphere encapsulated BSA for the respective tissue-specific layers. An interesting phenomenon was observed with regards to nHA-containing bone layer samples. A significant decrease in protein release was noted and is postulated to be attributed to electrostatic interactions between the negative carboxyl terminals of the globular protein and positively-charged species (H^+ and Ca^{2+}) of the nHA particles present at the material's surface as described by Tarafder et al.[51] Cartilage layer samples containing PLGA nanospheres exhibited similar release kinetics (Figure 6B) when compared to pure nanospheres (Figure 4B) with ~25% total protein released after 1 week of incubation.

A representative stress–strain curve of fabricated biphasic nanocomposite scaffolds is illustrated in Figure 7. The bimodal nature of the curve is reflective of the biphasic construct where region A (cartilage layer) and region B (bone layer) exhibit elastic moduli of 6.07 ± 0.170 MPa and 21.65 ± 1.91 MPa, respectively. The mechanical properties of the specimens tested exhibited elastic moduli similar to reported values[4] for cartilage and osteochondral tissue. The modular nature of the system allows for greater tunability through the use of alternative photocrosslinkable hydrogels (i.e., methacrylated PEG, polypropylene fumarate), as well as PEG derivatives of varying molecular weights. Both cartilage and bone layer compositions can be readily modified.

Figure 8 shows the 4 h cell adhesion study on bone layer scaffolds. The results show that cells attached more to 20% nHA than 10% or the 0% control. More importantly, the scaffolds containing PDO nanospheres and/or 20% nHA have the highest cell density, thus, suggesting the very good cytocompatibility properties of the fabricated nanocomposite scaffolds.

In the hMSC differentiation studies, the respective bone and cartilage layers of the osteochondral scaffold were evaluated for hMSC osteogenic and chondrogenic differentiation potential. Bone layer samples were evaluated for extracellular calcium deposition and total collagen production. The total calcium deposition (Figure 9) revealed greater calcium deposition in all nanocomposite samples after 1 and 2 weeks. In addition, although blended BMP-2 into nHA scaffolds had a higher calcium deposition after 1 week, BMP-2 encapsulated nanospheres and nHA scaffolds showed a statistically significant increase from week 1 to week 2.

Total collagen synthesis (Figure 10) increased in all nanostructured bone layer samples with respect to control after 2 weeks of culture. Although no distinguishable difference was observed after 1 week, after 2 weeks all nHA/BMP-2 PCL samples performed better than PCL control samples, as well as shown a statistically significant increase in collagen production when compared to week 1. Moreover, our results show that BMP-2 encapsulated PDO nanospheres can achieve the highest collagen synthesis when compared to BMP-2 blended and all other samples after 2 weeks. Although various growth factors (e.g., TGF-β1 and BMP-2)

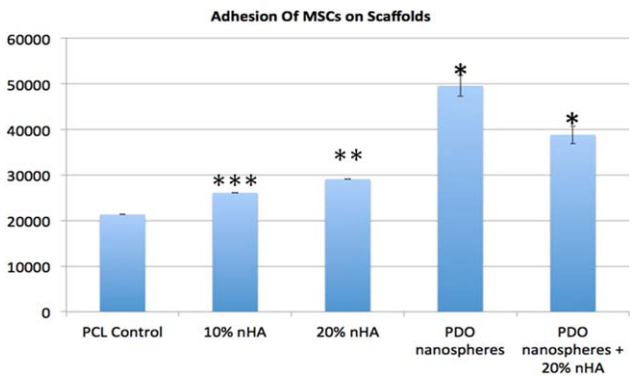

Figure 8. Enhanced hMSC adhesion on PCL scaffold with PDO nanosphere and 20% nHA, Data are mean ± StdEM, n = 9; $^{*}p<0.05$ when compared to all other samples; $^{**}p<0.05$ when compared to 10% nHA in PCL and PCL controls; $^{***}p<0.05$ when compared to PCL controls.

[Color figure can be viewed in the online issue, which is available at wileyonlinelibrary.com.]

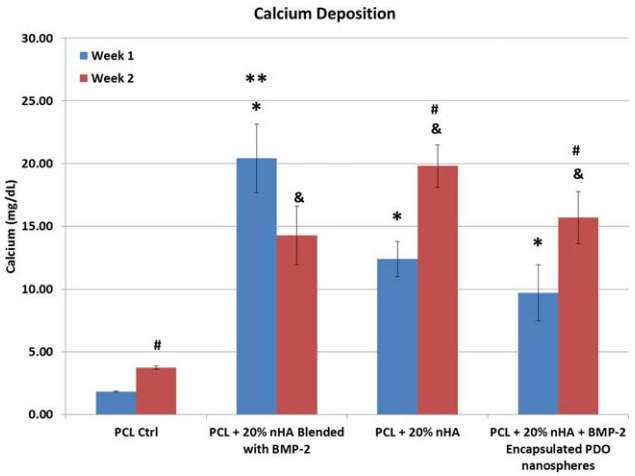

Figure 9. Calcium deposition of bone layer samples.

Data are mean ± StdEM, $n = 6$; $^{**}p<0.01$ when compared to all samples and $^{*}p<0.01$ when compared to controls after 1 week of culture. &$p<0.01$ when compared to controls after 2 weeks of culture and #$p<0.05$ when compared to respective scaffold in week 1. [Color figure can be viewed in the online issue, which is available at wileyonlinelibrary.com.]

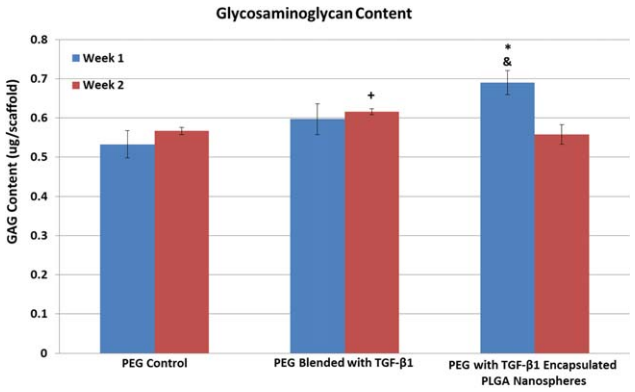

Figure 11. Total GAG content of cartilage layer samples.

Data are mean ± StdEM, n = 6; &$p<0.01$ when compared to week 1 control; $^{*}p<0.05$ when compared to week 2 sample; +$p<0.05$ when compared to all week 2 samples. [Color figure can be viewed in the online issue, which is available at wileyonlinelibrary.com.]

have been shown to improve MSC osteogenic or chondrogenic differentiation,[52–62] methods for administering them face ongoing issues with regards to short-term retention, quick half-life in circulation, and quick loss of biological activity even when administered at high-dose rates. When local delivery to the osteochondral defect site is employed, rapid diffusion to adjacent tissues and loss of bioactivity limits their potential to promote prolonged osteochondral tissue formation in the defect site. In our study, we designed a series of novel PDO nanospheres which can release BMP-2 in a sustained and controlled fashion, thus, potentially facilitating long-term tissue regeneration. Our osteogenic differentiation study has demonstrated that our nanostructured bone layer scaffold with nHA and BMP-2 encapsulated PDO nanospheres are promising for osteochondral tissue regeneration applications.

Biochemical analysis of 1 and 2 week chondrogenic hMSC differentiation showed PLGA nanosphere scaffolds with encapsulated TGF-β1 performed better than untreated control (Figures 11–13). Specifically, there was a significant increase in GAG content after 1 week (Figure 11). TGF-β1 has been shown to positively direct early and late-stage hMSC chondrogenic differentiation from initial increased GAG production to hypertrophic maturation of seeded hMSCs. Tezcan et al.[63] examined TGF-β1 induced MSC chondrogenic differentiation and correlated their findings as a dose-dependent response wherein TGF-β1 was critical in the initiation of GAG synthesis and late stage hypertrophy and maturation. The decrease in GAG synthesis on PLGA nanosphere cartilage samples may be attributed to this dose-dependent relation.

Figure 12 illustrates the total collagen synthesis in cartilage layer scaffolds. No statistical difference was observed among the experimental groups after 2 weeks. However, it was observed that both TGF-β1 containing samples had

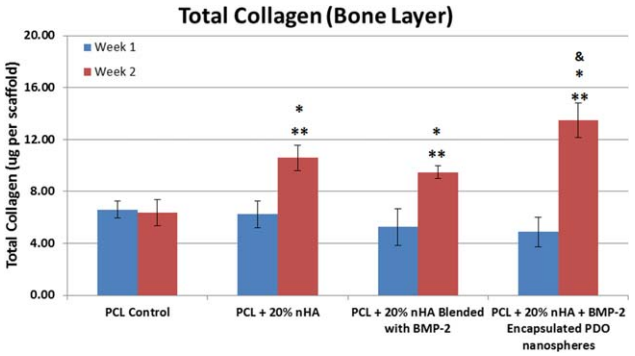

Figure 10. Significantly improved total collagen content in nanocomposite bone layer scaffolds after 2 week of culture.

Data are mean ± StdEM, n = 6; $^{*}p<0.01$ when compared to PCL control after 2 week and $^{**}p<0.05$ when compared to respective scaffolds in week 1. Nanosphere containing samples also showed greater collagen content with respect to BMP-2 blended samples (&$p<0.05$). [Color figure can be viewed in the online issue, which is available at wileyonlinelibrary.com.]

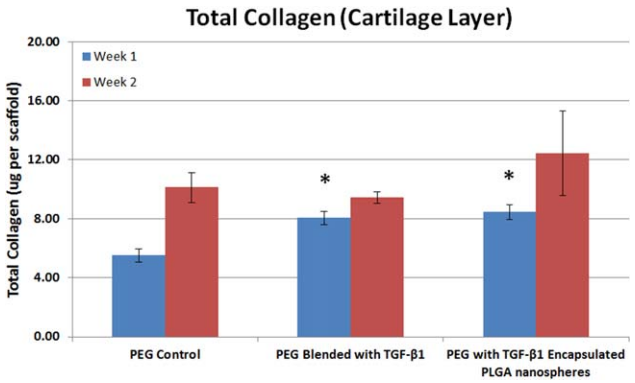

Figure 12. Total collagen content of cartilage layer samples.

Data are mean ± StdEM, $n = 6$; Both blended and nanosphere encapsulated TGF-β1 samples out performed control after 1 week ($^{*}p<0.01$). [Color figure can be viewed in the online issue, which is available at wileyonlinelibrary.com.]

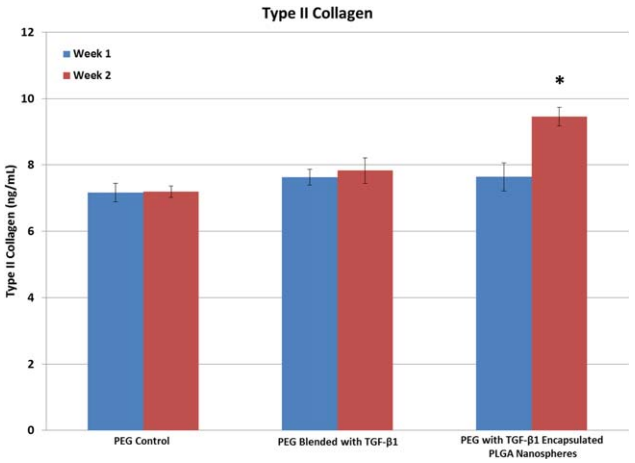

Figure 13. Type II collagen content of cartilage layer samples.

Data are mean ± StdEM, n = 6; nanosphere encapsulated TGF-bgr;1 samples out performed control after 1 week ($^{*}p<0.05$). [Color figure can be viewed in the online issue, which is available at wileyonlinelibrary.com.]

increased collagen synthesis when compared to control after 1 week of culture, which aided in promoting early cartilage formation. More importantly, type II collagen is a late-stage marker of chondrogenic differentiation which significantly increased after 2 weeks (Figure 13) for PLGA nanosphere scaffolds when compared to control and TGF-β1 blended scaffolds. All of these data reveal the great potential of novel TGF-β1 encapsulated PLGA nanosphere hydrogel scaffolds in improving chondrogenic differentiation of hMSCs.

Conclusions

The work presented herein served to illustrate the feasibility of manufacturing a novel biphasic osteochondral nanocomposite scaffold with controlled growth factor release. It differs from recently published work in the field wherein this work focused on modulating hMSC behavior via a biomimetic scaffold composed of biocompatible polymeric materials and bioactive nanobiomaterials. Novel aspects of this study include the development of an efficient wet electrospray technique to manufacture growth factor encapsulated core–shell nanospheres in addition to co-porogen UV crosslinking of two disparate polymeric materials. hMSC adhesion and osteochondral differentiation were enhanced through the incorporation of tissue-specific nanomaterials including nHA, BMP-2-loaded PDO and TGF-β1-loaded PLGA nanospheres. Due to the nature of the model, additional growth factor encapsulated spheres can be readily incorporated and evaluated for neovascularization. The current biphasic osteochondral model and nanosphere fabrication method hold great potential for orthopedic tissue engineering applications.

Acknowledgments

The authors would like to thank Research Award from the Clinical and Translational Science Institute at Children's National (CTSI—CN) and support from the George Washington University Institute for Nanotechnology (GWIN) and the George Washington Institute for Biomedical Engineering (GWIBE). This contribution was identified as the Best Presentation in the session "Nanostructured Scaffolds for Tissue Engineering" of the 2012 AICHE Annual Meeting in Pittsburgh, PA.

Literature Cited

1. Lawrence RC, Felson DT, Helmick CG, et al. Estimates of the prevalence of arthritis and other rheumatic conditions in the United States. Part II. *Arthritis Rheum*. 2008;58(1):26–35.
2. National Center for Chronic Disease Prevention and Health Promotion; 2008. http://www.cdc.gov/arthritis/arthritis/osteoarthritis.htm. Accessed September 1st, 2009.
3. Castro NJ, Hacking SA, Zhang LG. Recent progress in interfacial tissue engineering approaches for osteochondral defects. *Ann Biomed Eng*. 2012;40(8):1628–1640.
4. Zhang L, Hu J, Kyriacos A. Athanasiou. The role of tissue engineering in articular cartilage repair and regeneration. *Crit Rev Biomed Eng*. 2009;37(1-2):1–57.
5. Holmes B, Castro NJ, Zhang LG, Zussman E. Electrospun fibrous scaffolds for cartilage and bone regeneration: recent progress and future developments. *Tissue Eng Part B Rev*. 2012;18(6):478–486.
6. Temenoff JS, Yang PJ. Engineering orthopedic tissue interfaces. *Tissue Eng Part B*. 2009;15(2):127–141.
7. Nooeaid P, Salih V, Beier JP, Boccaccini AR. Osteochondral tissue engineering: scaffolds, stem cells and applications. *J Cell Mol Med*. 2012;16(10):2247–2270.
8. Bal BS, Rahaman MN, Jayabalan P, et al. In vivo outcomes of tissue-engineered osteochondral grafts. *J Biomed Mater Res Part B*. 2010;93(1):164–174.
9. Im GI, Ahn JH, Kim SY, Choi BS, Lee SW. A hyaluronate-atelocollagen/beta-tricalcium phosphate-hydroxyapatite biphasic scaffold for the repair of osteochondral defects: a porcine study. *Tissue Eng Part A*. 2010;16(4):1189–1200.
10. Mohan N, Dormer NH, Caldwell KL, Key VH, Berkland CJ, Detamore MS. Continuous gradients of material composition and growth factors for effective regeneration of the osteochondral interface. *Tissue Eng Part A*. 2011;17(21-22):2845–2855.
11. Dormer NH, Singh M, Zhao L, Mohan N, Berkland CJ, Detamore MS. Osteochondral interface regeneration of the rabbit knee with macroscopic gradients of bioactive signals. *J Biomed Mater Res A*. 2012;100A(1):162–170.
12. Dormer NH, Qiu Y, Lydick AM, et al. Osteogenic differentiation of human bone marrow stromal cells in hydroxyapatite-loaded microsphere-based scaffolds. *Tissue Eng Part A*. 2012;18(7-8):757–767.
13. Zhang L, Li JY, Lee JD. Nanotechnology for cartilage and bone regeneration. In: Webster TJ, ed. *Nanomedicine: Technologies and Applications*. Cambridge, UK: Woodhead Publishing Ltd; 2012:571–598.
14. Zhang L, Webster TJ. Nanotechnology and nanomaterials: Promises for improved tissue regeneration. *Nanotoday*. 2009;4(1):66–80.
15. Filova E, Rampichova M, Litvinec A, et al. A cell-free nanofiber composite scaffold regenerated osteochondral defects in miniature pigs. *Int J Pharm*. 2013;447(1-2):139–149.
16. Salerno A, Iannace S, Netti PA. Graded biomimetic osteochondral scaffold prepared via CO2 foaming and micronized NaCl leaching. *Mater Lett*. 2012;82:137–140.
17. Christensen BB, Foldager CB, Hansen OM, et al. A novel nanostructured porous polycaprolactone scaffold improves hyaline cartilage repair in a rabbit model compared to a collagen type I/III scaffold: in vitro and in vivo studies. Knee surgery, sports traumatology, arthroscopy. *Official journal of the ESSKA*. 2012;20(6):1192–1204.
18. Zhang L, Huang J, Si T, Xu RX. Coaxial electrospray of microparticles and nanoparticles for biomedical applications. *Expert Rev Med Devic*. 2012;9(6):595–612.
19. Lim JJ, Hammoudi TM, Bratt-Leal AM, et al. Development of nano- and microscale chondroitin sulfate particles for controlled growth factor delivery. *Acta Biomater*. 2011;7(3):986–995.
20. Im O, Li J, Wang M, Zhang LG, Keidar M. Biomimetic three-dimensional nanocrystalline hydroxyapatite and magnetically synthesized single-walled carbon nanotube chitosan nanocomposite for bone regeneration. *Int J Nanomedicine*. 2012;7:2087–2099.
21. Zhang L, Rodriguez J, Raez J, Myles AJ, Fenniri H, Webster TJ. Biologically inspired rosette nanotubes and nanocrystalline hydroxyapatite hydrogel nanocomposites as improved bone substitutes. *Nanotechnology*. 2009;20(17):175101.
22. Sun L, Zhang L, Hemraz UD, Fenniri H, Webster TJ. Bioactive rosette nanotube-hydroxyapatite nanocomposites improve osteoblast functions. *Tissue Eng Part A*. 2012;18(17-18):1741–1750.
23. Arcaute K, Mann BK, Wicker RB. Stereolithography of three-dimensional bioactive poly(ethylene glycol) constructs with encapsulated cells. *Ann Biomed Eng*. 2006;34(9):1429–1441.
24. Colter DC, Class R, DiGirolamo CM, Prockop DJ. Rapid expansion of recycling stem cells in cultures of plastic-adherent cells from

human bone marrow. *Proc Natl Acad Sci USA*. 2000;97(7):3213–3218.
25. de Boer R, Knight AM, Spinner RJ, Malessy MJ, Yaszemski MJ, Windebank AJ. In vitro and in vivo release of nerve growth factor from biodegradable poly-lactic-*co*-glycolic-acid microspheres. *J Biomed Mater Res A*. 2010;95(4):1067–1073.
26. Dawes GJ, Fratila-Apachitei LE, Necula BS, Apachitei I, Witkamp GJ, Duszczyk J. Release of PLGA-encapsulated dexamethasone from microsphere loaded porous surfaces. *J Mater Sci*. 2010;21(1):215–221.
27. Dawes GJ, Fratila-Apachitei LE, Mulia K, Apachitei I, Witkamp GJ, Duszczyk J. Size effect of PLGA spheres on drug loading efficiency and release profiles. *J Mater Sci*. 2009;20(5):1089–1094.
28. Hwang YK, Jeong U, Cho EC. Production of uniform-sized polymer core–shell microcapsules by coaxial electrospraying. *Langmuir*. 2008;24(6):2446–2451.
29. Enayati M, Ahmad Z, Stride E, Edirisinghe M. One-step electrohydrodynamic production of drug-loaded micro- and nanoparticles. *J R Soc Interface*. 2010;7(45):667–675.
30. Enayati M, Ahmad Z, Stride E, Edirisinghe M. Size mapping of electric field-assisted production of polycaprolactone particles. *J R Soc Interface*. 2010;7:S393–S402.
31. Thomas V, Zhang X, Vohra YK. A biomimetic tubular scaffold with spatially designed nanofibers of protein/PDS bio-blends. *Biotechnol Bioeng*. 2009;104(5):1025–1033.
32. Venclauskas L, Grubinskas I, Mocevicius P, Kiudelis M. Reinforced tension line versus simple suture: a biomechanical study on cadavers. *Acta Chir Belg*. 2011;111(5):288–292.
33. Sakamoto A, Kiyokawa K, Rikimaru H, Watanabe K, Nishi Y. An investigation of the fixation materials for cartilage frames in microtia. *J Plast Reconstr Aesthet Surg*. 2012;65(5):584–589.
34. Almeria B, Deng W, Fahmy TM, Gomez A. Controlling the morphology of electrospray-generated PLGA microparticles for drug delivery. *J Colloid Interface Sci*. 2010;343(1):125–133.
35. Panusa A, Selmin F, Rossoni G, Carini M, Cilurzo F, Aldini G. Methylprednisolone-loaded PLGA microspheres: a new formulation for sustained release via intra-articular administration. A comparison study with methylprednisolone acetate in rats. *J Pharm Sci*. 2011;100(11):4580–4586.
36. Stevanovic M, Uskokovic D. Poly(lactide-*co*-glycolide)-based micro and nanoparticles for the controlled drug delivery of vitamins. *Curr Nanosci*. 2009;5(1):1–14.
37. Zhu J, Dang HC, Wang WT, Wang XL, Wang YZ. Cellulose diacetate-*g*-poly(p-dioxanone) co-polymer: synthesis, properties and microsphere preparation. *J Biomater Sci Polym Ed*. 2011;22(8):981–999.
38. Wang XL, Chen YY, Wang YZ. Synthesis of poly(p-dioxanone) catalyzed by Zn L-lactate under microwave irradiation and its application in ibuprofen delivery. *J Biomater Sci Polym Ed*. 2010;21(6):927–936.
39. Madurantakam PA, Rodriguez IA, Cost CP, et al. Multiple factor interactions in biomimetic mineralization of electrospun scaffolds. *Biomaterials*. 2009;30(29):5456–5464.
40. Smith MJ, McClure MJ, Sell SA, et al. Suture-reinforced electrospun polydioxanone-elastin small-diameter tubes for use in vascular tissue engineering: a feasibility study. *Acta Biomater*. 2008;4(1):58–66.
41. Kalfa D, Bel A, Chen-Tournoux A, et al. A polydioxanone electrospun valved patch to replace the right ventricular outflow tract in a growing lamb model. *Biomaterials*. 2010;31(14):4056–4063.
42. Bouffi C, Thomas O, Bony C, et al. The role of pharmacologically active microcarriers releasing TGF-beta3 in cartilage formation in vivo by mesenchymal stem cells. *Biomaterials*. 2010;31(25):6485–6493.
43. Elisseeff J, McIntosh W, Fu K, Blunk BT, Langer R. Controlled-release of IGF-I and TGF-beta1 in a photopolymerizing hydrogel for cartilage tissue engineering. *J Orthop Res*. 2001;19(6):1098–1104.
44. Graves RA, Poole D, Moiseyev R, Bostanian LA, Mandal TK. Encapsulation of indomethacin using coaxial ultrasonic atomization followed by solvent evaporation. *Drug Dev Ind Pharm*. 2008;34(4):419–426.
45. Solorio LD, Fu AS, Hernandez-Irizarry R, Alsberg E. Chondrogenic differentiation of human mesenchymal stem cell aggregates via controlled release of TGF-beta1 from incorporated polymer microspheres. *J Biomed Mater Res A*. 2010;92(3):1139–1144.
46. Verreck G, Chun I, Li Y, et al. Preparation and physicochemical characterization of biodegradable nerve guides containing the nerve growth agent sabeluzole. *Biomaterials*. 2005;26(11):1307–1315.
47. Liu J, Jiang Z, Zhang S, et al. Biodegradation, biocompatibility, and drug delivery in poly(ω-pentadecalactone-*co*-p-dioxanone) copolyesters. *Biomaterials*. 2011;32(27):6646–6654.
48. Zhang L, Feng Y, Tian H, Shi C, Zhao M, Guo J. Controlled release of doxorubicin from amphiphilic depsipeptide-PDO-PEG-based copolymer nanosized microspheres. *React Funct Polym*. 2013;73(9):1281–1289.
49. Wang M, Castro NJ, Li J, Keidar M, Zhang LG. Greater osteoblast and mesenchymal stem cell adhesion and proliferation on titanium with hydrothermally treated nanocrystalline hydroxyapatite/magnetically treated carbon nanotubes. *J Nanosci Nanotechnol*. 2012;12(10):7692–7702.
50. Sato M, Aslani A, Sambito MA, Kalkhoran NM, Slamovich EB, Webster TJ. Nanocrystalline hydroxyapatite/titania coatings on titanium improves osteoblast adhesion. *J Biomed Mater Res A*. 2008;84A(1):265–272.
51. Tarafder S, Banerjee S, Bandyopadhyay A, Bose S. Electrically polarized biphasic calcium phosphates: adsorption and release of bovine serum albumin. *Langmuir*. 2010;26(22):16625–16629.
52. Noel D, Gazit D, Bouquet C, et al. Short-term BMP-2 expression is sufficient for in vivo osteochondral differentiation of mesenchymal stem cells. *Stem Cells*. 2004;22(1):74–85.
53. Sekiya I, Colter DC, Prockop DJ. BMP-6 enhances chondrogenesis in a subpopulation of human marrow stromal cells. *Biochem Biophys Res Commun*. 2001;284(2):411–418.
54. Bai X, Li G, Zhao C, Duan H, Qu F. BMP7 induces the differentiation of bone marrow-derived mesenchymal cells into chondrocytes. *Med Biol Eng Comput*. 2011;49(6):687–692.
55. Chim H, Miller E, Gliniak C, Alsberg E. Stromal-cell-derived factor (SDF) 1-alpha in combination with BMP-2 and TGF-beta1 induces site-directed cell homing and osteogenic and chondrogenic differentiation for tissue engineering without the requirement for cell seeding. *Cell Tissue Res*. 2012;350(1):89–94.
56. Kim M, Erickson IE, Choudhury M, Pleshko N, Mauck RL. Transient exposure to TGF-beta3 improves the functional chondrogenesis of MSC-laden hyaluronic acid hydrogels. *J Mech Behav Biomed Mater*. 2012;11:92–101.
57. Ertan AB, Yilgor P, Bayyurt B, et al. Effect of double growth factor release on cartilage tissue engineering. *J Tissue Eng Reg Med*. 2013;7(2):149–160.
58. Kwon SH, Lee TJ, Park J, et al. Modulation of BMP-2-induced chondrogenic versus osteogenic differentiation of human mesenchymal stem cells by cell-specific extracellular matrices. *Tissue Eng Part A*. 2013;19(1-2):49–58.
59. Davis HE, Case EM, Miller SL, Genetos DC, Leach JK. Osteogenic Response to BMP-2 of hMSCs grown on apatite-coated scaffolds. *Biotechnol Bioeng*. 2011;108(11):2727–2735.
60. Huang WB, Carlsen B, Wulur I, et al. BMP-2 exerts differential effects on differentiation of rabbit bone marrow stromal cells grown in two-dimensional and three-dimensional systems and is required for in vitro bone formation in a PLGA scaffold. *Exp Cell Res*. 2004;299(2):325–334.
61. Kim J, Kim IS, Cho TH, et al. Bone regeneration using hyaluronic acid-based hydrogel with bone morphogenic protein-2 and human mesenchymal stem cells. *Biomaterials*. 2007;28(10):1830–1837.
62. Kim SE, Rha HK, Surendran S, et al. Bone morphogenic protein-2 (BMP-2) immobilized biodegradable scaffolds for bone tissue engineering. *Macromol Res*. 2006;14(5):565–572.
63. Tezcan B, Serter S, Kiter E, Tufan AC. Dose dependent effect of C-type natriuretic peptide signaling in glycosaminoglycan synthesis during TGF-beta1 induced chondrogenic differentiation of mesenchymal stem cells. *J Mol Histology*. 2010;41(4-5):247–258.

Manuscript received Mar. 11, 2013, and revision received Oct. 10, 2013.